*Journal of Zhejiang University-SCIENCE B (Biomedicine & Biotechnology) in press*
www.jzus.zju.edu.cn; www.springer.com/journal/11585
E-mail: jzus_b@zju.edu.cn

**Research Article**

https://doi.org/10.1631/jzus.B2300825

# Pharmacological inhibition of ENaC or NCX can attenuate hepatic ischemia-reperfusion injury exacerbated by hypernatremia

Yabin CHEN[1], Hao LI[2], Peihao WEN[1], Jiakai ZHANG[1], Zhihui WANG[1], Shengli CAO[1], Wenzhi GUO[1]✉

[1]*Department of Hepatobiliary and Pancreatic Surgery, The First Affiliated Hospital of Zhengzhou University, Zhengzhou, Henan, 450052, China*
[2]*Henan Organ Transplantation Centre, Zhengzhou, Henan, 450052, China*

**Abstract:** Donors with serum sodium concentration >155 mmol/L are extended criteria donors for liver transplantation (LT). Elevated serum sodium of donors leads to an increased incidence of hepatic dysfunction in the early postoperative period of LT; the exact mechanism has not been reported. We constructed a Lewis rat model of 70% hepatic ischemia-reperfusion (I/R) with hypernatremia and a BRL-3A cell model of hypoxia-reoxygenation (H/R) with high sodium concentration (HS) culture medium precondition. To determine the degree of injury, biochemical analysis, histological analysis, and oxidative stress and apoptosis detection were performed. We applied specific inhibitors of the epithelial sodium channel (ENaC) and $Na^+/Ca^{2+}$ exchanger (NCX) in vivo and in vitro to verify their role in injury. Serum alanine aminotransferase (ALT), aspartate aminotransferase (AST), and lactate dehydrogenase (LDH) levels and the area of hepatic necrosis were significantly elevated in the HS + I/R group. Increased reactive oxygen species (ROS) production, MPO-positive cells, and aggravated cellular apoptosis were seen in the HS + I/R group. The HS + H/R group of BRL-3A cells showed significantly increased cellular apoptosis and ROS production compared to the H/R group. The application of Amiloride (Amil), a specific inhibitor of ENaC, reduced ischemia-reperfusion injury (IRI) aggravated by HS both in vivo and in vitro, evidenced by decreased serum transaminases, inflammatory cytokines, apoptosis, and oxidative stress. SN-6, a specific inhibitor of NCX, had a similar effect. In summary, hypernatremia aggravates hepatic ischemia-reperfusion injury (IRI), which can be attenuated by pharmacological inhibition of ENaC or NCX.

**Key words:** Liver transplantation; Epithelial sodium channel; Sodium/calcium exchanger; Hypernatremia



## 1 Introduction

Liver transplantation (LT) is an effective treatment for various end-stage liver diseases, and the livers are mainly derived from brain-dead donors (Guo et al., 2023; Schlegel et al., 2023). Shortage of donor livers is one of the dilemmas facing LT, and expanding the source of donor livers has become critical, with more and more extended-criteria donor livers being used in transplantation (Ceresa et al., 2022; Sitbon et al., 2023). Extended-criteria donor livers are those with a high risk of primary graft nonfunction or hypofunction and delayed graft inactivation after transplantation. A donor with serum sodium concentration >155 mmol/L (hypernatremia donors) would be considered an extended-criteria donor (Basmaji et al., 2020; Lin et al., 2023). It has been proven that the use of livers from hypernatremia donors leads to an increased incidence of poor liver function in the short-term postoperative period, and some studies also have reported elevated postoperative mortality of recipients (Bastos-Neves et al., 2019; Basmaji, et al., 2020; Zhou et al., 2020; Mcdonald et al., 2021).

✉ Wenzhi GUO, fccguowz@zzu.edu.cn
Wenzhi GUO, https://orcid.org/0000-0002-0821-1318

Received Nov. 14, 2023; Revision accepted Apr. 22, 2024
Crosschecked xxx. xx, 20xx; Published online xxx. xx, 20xx

Ischemia-reperfusion injury (IRI) is an important cause of postoperative hepatic dysfunction. During periods of liver ischemia, the lack of oxygen and energy supply to hepatocytes leads to metabolic abnormalities and the release of danger-associated molecular patterns (DAMPs) (Kaltenmeier et al., 2022; Lucas-Ruiz et al., 2023). After the blood supply is restored, the improved oxygen supply increases the production of reactive oxygen species (ROS), which further aggravates cellular damage and inflammatory responses (Dar et al., 2019). However, the mechanism by which hypernatremia aggravates hepatic IRI has not been reported.

ENaC is a kind of sodium channel that is widely distributed in multiple organs, and mainly mediates cellular sodium transport (Chen et al., 2023). Hypernatremia aggravates renal IRI through ENaC. Amil can reduce the expression of ENaC and attenuate hypernatremia-aggravated renal IRI (Matsumoto et al., 2022). The expression of $Na^+$-$Ca^{2+}$ exchanger (NCX) is increased after myocardial IR, and SN-6 can decrease the expression of NCX and be applied to reduce myocardial IRI (Castaldo et al., 2017). Activation of the ENaC-NCX-NLRP3 signaling pathway can lead to increased ROS production and exacerbated inflammatory responses, which have been reported in many diseases such as cystic fibrosis (Scambler et al., 2019) and salt-sensitive hypertension (Chen et al., 2021; Pitzer et al., 2022). Therefore, we hypothesized that hypernatremia aggravates hepatic IRI is association with the activation of ENaC and NCX.

## 2 Materials and methods

### 2.1 Animals

Male Lewis rats (6–8 weeks) were purchased from Beijing Viton Lihua Laboratory Animal Technology Co. All rats were housed in 25 ± 2 ℃ and 55 ± 5% humidity environment with a 12-h dark/light cycle. All rats were acclimatized for 1 week prior to the experiment.

### 2.2 Rat models and drug treatment

For the I/R rat model, a 70% liver warm ischemia model was established as previously described. Briefly, Lewis rats were anesthetized with sodium pentobarbital, and the abdominal wall was clipped longitudinally. The arteries, portal veins, and bile ducts of the left and middle lobes of the livers were clamped with vascular clips for 1 h, followed by reperfusion for 6 h. Then, the rats were sacrificed, and specimens were obtained (Guo et al., 2020; Li et al., 2023).

For the high sodium concentration (HS) rat model, Lewis rats were anesthetized, and a high-sodium solution was pumped via tail vein cannulation. Firstly, 0.7 ml per 100 g body weight of 3 mol/L NaCl solution was rapidly pumped over 5 min. Then, 0.7 ml/h of 3 mol/L NaCl solution was continuously pumped for 3 h, followed by 0.2 ml/h continuously pumped for 6 h. Blood was drawn intermittently via femoral artery cannulation for the detection of serum sodium concentration.

For the HS + I/R rat model, the pumping of the high-sodium solution was stopped after the establishment of the HS rat model, and then the establishment of the I/R model was continued with intermittent oral feeding of a 20% glucose solution and subcutaneous injection of sodium pentobarbital.

For the Amil + I/R rat model, prior to the establishment of the I/R model, rats were injected intraperitoneally with 1 mg Amil (HY-B0285A, MedChemExpress, USA) per 1 kg body weight (Quansah and N'gouemo, 2014; Frindt et al., 2018). The SN-6 + I/R rat model was established in the same way, with 1 mg SN-6 (HY-107658, MedChemExpress, USA) per 1 kg body weight (N'gouemo, 2013; Quansah and N'gouemo, 2014; Persaud et al., 2022). For the Amil + HS + I/R rat model, rats were injected intraperitoneally with 1 mg/kg Amil prior to the establishment of the HS + I/R model, while the SN-6 + HS + I/R rat model was established in the same way with 1 mg/kg SN-6.

### 2.3 Cell culture and cell models

BRL-3A cells (Cellverse, Shanghai, China) were cultured with Dulbecco's Modified Eagle Medium

(DMEM, Solarbio, Beijing, China) added to 10% fetal bovine serum (Gibco, CA, USA) in normal conditions (5% CO2/water-saturated incubator at 37 ℃). For the HS cell model, the sodium concentration of the culture medium was 190 mmol/L.

For the H/R cell model, the medium was changed to serum-free and glucose-free DMEM, and the cells were transferred to a modular incubator chamber (Biospherix, Lacona, NY, USA) under hypoxic conditions (1% O2, 5% CO2, and 94% N2). After 6 h of hypoxia, the cells were transferred into a normoxic incubator (95% air + 5%CO2 mixture) for reoxygenation for 6h, and the medium was changed to a complete medium. For the HS + H/R cell model, the cells were first cultured in 190 mmol/L culture medium for several hours, followed by H/R conditions (Guo, et al., 2020; Ding et al., 2022).

For the Amil + H/R cell model, the cells were first cultured in a culture medium containing 10μM Amil, followed by H/R conditions, while the SN-6 + H/R cell model was established with 10μM SN-6. For the Amil + HS + H/R cell model, the cells were first cultured in 190 mmol/L culture medium containing 10μM Amil, followed by H/R conditions, while the SN-6 + HS + H/R cell model was established with 10μM SN-6.

### 2.4 Biochemical analysis

ALT, AST, and LDH in the serum of the rats were tested using commercial kits (JianCheng Bioengineering Institute, Nanjing, China) according to the manufacturer's instructions.

### 2.5 Cell counting kit-8 (CCK-8) assay

BRL-3A cells were inoculated into 96-well plates at a cell density of $5 \times 10^3$ cells/well, and subjected to different treatments followed by H/R. Then, according to the instructions of the CCK-8 kit, 10 μL of CCK-8 reagent (Boster, Wuhan, China) was added to each well. The absorbance of each well was detected at 450 nm after being incubated for 1 h at 37 °C.

### 2.6 Histological and immunohistochemical staining

All hepatic tissues were fixed in 10% formaldehyde solution and embedded in paraffin. Then, the tissues were cut into 5 μm sections. Paraffin sections were stained with hematoxylin and eosin (Servicebio, Wuhan, China) for H&E staining. MPO (1:100) antibody (Servicebio, Wuhan, China) and secondary antibody (1:200) (Servicebio, Wuhan, China) were incubated for immunohistochemical staining. The images were photographed using an inverted optical microscope (Olympus, Tokyo, Japan).

### 2.7 Flow cytometry analysis

After discarding the medium, the BRL-3A cells were washed twice with phosphate buffered saline (PBS), then digested with EDTA-free trypsin (Beyotime, Shanghai, China), collected, and centrifuged at 200 g for 5 min. Next, 100 μL binding buffer, 5 μL AnnexinV-FITC, and 5 μL propidium iodide (Beyotime, Shanghai, China) were added to resuspend the cells, before incubating them at room temperature for 15 min in the dark, finally detecting them using flow cytometry.

### 2.8 Western blot analysis

Protein expression levels in hepatic tissues and cells were detected by Western blot analysis according to standard protocols. RIPA reagent (Solarbio, Beijing, China) was used to extract proteins and a BCA kit (Solarbio, Beijing, China) was used to quantify the concentrations of proteins. The proteins were separated by 10% or 12% sodium dodecyl sulphate-polyacrylamide gel electrophoresis (SDS-PAGE), then transferred to PVDF membranes. The PVDF membranes were incubated with the specific primary antibody at 4 °C overnight, followed by secondary antibody at 37 °C for 1 h. All the antibodies' information is listed in Supplementary Table 1. The ECL chemiluminescence reagent (NCM Biotech, Suzhou, China) was used, and the signals were detected using the ChemiDoc™ MP Imaging System (BioRad, Hercules, CA, USA).

### 2.9 Quantitative real-time (RT)-PCR

Trizol reagent (Invitrogen, Carlsbad, CA, USA) was used to extract total RNA from the hepatic tissues and BRL-3A cells. After reverse transcription of the RNA to cDNA, quantitative RT-PCR was performed based on the instructions of SYBR qPCR Master Mix reagent (Vazyme, Nanjing, China). GAPDH was used as an internal reference gene; the primers used to amplify target gene fragments are listed in Supplementary Table 2.

### 2.10 Oxidative stress analysis

Hepatic tissue specimens were rapidly frozen and fixed; then, specimens were cut into 10 μm sections and stained with 10 μM dihydroethidium (DHE) fluorescent probe (Servicebio, Wuhan, China) and DAPI (Servicebio, Wuhan, China), respectively. After grinding the hepatic tissues, the protein concentration was determined by BCA, and the levels of MDA, SOD, and GSH (Solarbio, Beijing, China) in the tissues were determined according to the instructions. After removing the medium and washing the cells twice with PBS, ROS (Biosharp, Hefei, China) and DAPI were added to the BRL-3A cells according to the instructions and were photographed using a fluorescence microscope (Olympus, Tokyo, Japan).

### 2.11 Terminal deoxynucleotidyl transferase dUTP nick-end labeling (TUNEL) assay

Paraffin-embedded hepatic tissues were cut into 5μm-thick sections and then stained according to the instructions of the TUNEL kit (Servicebio, Wuhan, China). DAPI (Servicebio, Wuhan, China) was applied to stain the nucleus in the sections, followed by the application of an anti-fluorescence quenching solution (Servicebio, Wuhan, China). The images were photographed using a fluorescence microscope (Olympus, Tokyo, Japan).

### 2.12 Statistical analysis

All data were analyzed using SPSS software (version 27.0), expressed as mean ± standard deviation. The student's *t*-test was used to compare two groups, while one-way analysis of variance (ANOVA) was used to compare multiple groups. $P < 0.05$ was considered statistical significance. Levels of statistical significance were indicated as $*P < 0.05$, $**P < 0.01$, and $***P < 0.001$.



## 3 Results

### 3.1 Hypernatremia aggravates hepatic IRI in Lewis rats.

To study the effect of hypernatremia on hepatic I/R, we constructed a Lewis rat HS + I/R model by intravenously pumping 3 mol/L NaCl and using 70% of liver I/R (Fig.1A). Serum results showed that the ALT, AST, and LDH levels of rats in the HS + I/R group were significantly higher than those in the I/R group (Fig.1B-D), and the hepatic necrotic area in the HS + I/R group was significantly larger as shown in the H&E-stained images (Fig.1E-F). We further examined the infiltration of inflammatory cells and the expression of inflammatory cytokines in the liver. Immunohistochemical staining showed that MPO-positive inflammatory cells' infiltration was significantly increased in the HS + I/R group (Fig.1G-H). PCR results showed that the inflammatory cytokines IL-1β, MCP-1, and TNF-α were significantly elevated in the HS + I/R group (Fig.1J-L).

Hypernatremia also aggravated hepatocyte apoptosis after IRI. Western blot analysis showed that the expression of pro-apoptotic proteins BAX and C-Caspase 3 was remarkably increased in the HS + I/R group, while the expression of anti-apoptotic protein BCL-2 was decreased (Fig.1I). TUNEL staining showed that the number of apoptotic cells was significantly higher in the HS + I/R group than in the I/R group (Fig.1M-N). In order to detect the levels of ROS in hepatic tissues, we performed DHE staining, which showed that the number of positive cells in the HS + I/R group was significantly higher than that in the other groups (Fig.1O-P). GSH and SOD activity was significantly decreased in the HS + I/R group, whereas the MDA content was significantly elevated (Fig.1Q-S). Thus, these results suggest that hypernatremia exacerbates hepatic IRI in Lewis rats.

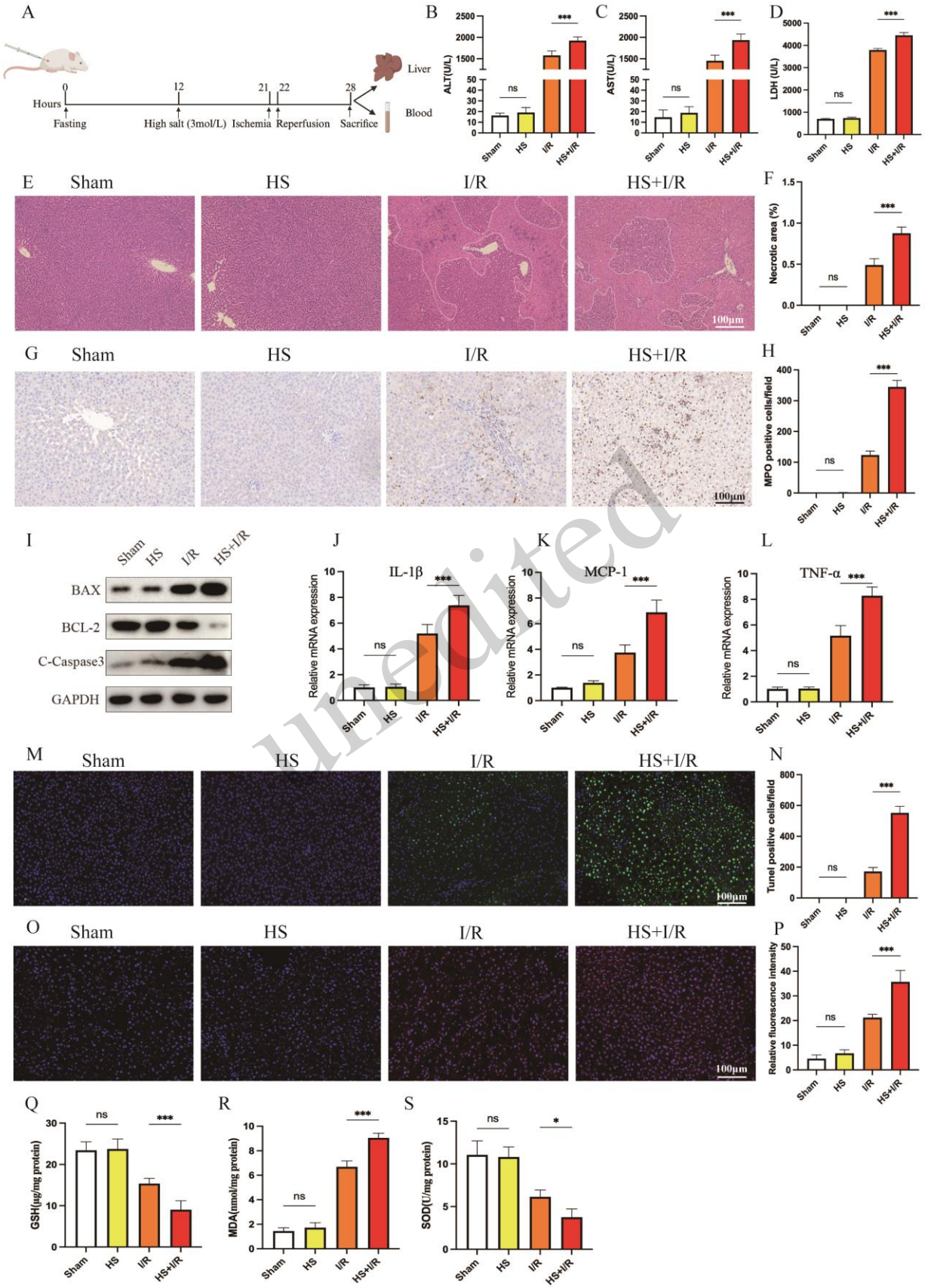
A
Hours
0
12
21
22
28
Fasting
High salt (3mol/L)
Ischemia
Reperfusion
Sacrifice
Liver
Blood
B
ALT(U/L)
C
AST(U/L)
D
LDH (U/L)
E
Sham
HS
I/R
HS+I/R
100μm
F
Necrotic area (%)
G
Sham
HS
I/R
HS+I/R
100μm
H
MPO positive cells/field
I
Sham
HS
I/R
HS+I/R
BAX
BCL-2
C-Caspase3
GAPDH
J
IL-1β
Relative mRNA expression
K
MCP-1
Relative mRNA expression
L
TNF-α
Relative mRNA expression
M
Sham
HS
I/R
HS+I/R
100μm
N
Tunel positive cells/field
O
Sham
HS
I/R
HS+I/R
100μm
P
Relative fluorescence intensity
Q
GSH(μg/mg protein)
R
MDA(nmol/mg protein)
S
SOD(U/mg protein)
ns
*
***

**Fig. 1 Hypernatremia aggravates hepatic IRI in Lewis rats. (A) Flow chart for the construction of the Lewis rat I/R model of hypernatremia. (B-D) Serum ALT, AST, LDH levels in rats of sham, HS, I/R, and HS + I/R groups (n=6/per group). (E) Representative hepatic H&E-stained images and (F) statistical charts (n=4/per group) showing necrotic areas, scale bar, 100 μm. (G) Representative hepatic MPO immunohistochemical staining images and (H) statistical charts (n=4/per group), scale bar, 100 μm. (I) The protein expression of BAX, BCL-2, and C-Caspase 3 in hepatic tissues. (J-L) The mRNA levels of IL-1β, MCP-1, and TNF-α in hepatic tissues. (M) Representative hepatic TUNEL staining images and (N) statistical charts (n=4/per group), scale bar, 100 μm. (O) Representative hepatic DHE staining images and (P) statistical charts (n=4/per group), scale bar, 100 μm. (Q-S) Hepatic GSH activity, MDA content, and SOD activity in sham, HS, I/R, and HS + I/R groups (n=6/per group).**

### 3.2 HS aggravates H/R injury in BRL-3A cells.

To investigate the effect of HS on the H/R of hepatocytes, we constructed a cell model of HS + H/R by placing BRL-3A cells into 190 mmol/L DMEM for 24 h then hypoxia for 6 h and reperfusion for 6 h (Fig.2A). CCK8 results showed that BRL-3A cells pretreated with HS before H/R decreased cell viability, which was most obvious with HS pretreatment for 24 h (Fig.2B). HS aggravated the apoptosis of hepatocytes after H/R; the flow cytometry results showed that the apoptosis rates of the cells were significantly increased after HS + H/R treatment (Fig.2C-D). Western blot results showed that the expression of BAX and C-Caspase 3 was significantly increased in the HS + H/R group, while the expression of BCL-2 was markedly decreased (Fig.2E). The fluorescence intensity of the ROS staining of the BRL-3A cells was elevated after H/R treatment, and the elevated fluorescence intensity of ROS staining was more obvious in the HS + H/R group (Fig.2F-G). In conclusion, these results demonstrated that HS aggravates the damage caused by H/R in BRL-3A cells.

### 3.3 Amil attenuates hypernatremia aggravated hepatic IRI in Lewis rats.

To investigate the role of ENaC in hypernatremia-exacerbated IRI, we added Amil by intraperitoneal injection into rat models of I/R and HS + I/R. The serum results showed that the ALT, AST, and LDH levels of rats in the Amil + HS + I/R group were significantly lower than those in the HS + I/R group (Fig.3A-C). The area of hepatic necrosis in the Amil + HS + I/R group was significantly smaller than that in the HS + I/R group, as seen in H&E-stained images (Fig.3D-E). Amil alleviated hypernatremia-induced hepatic I/R injury while also reducing hepatic inflammation. Immunohistochemical staining showed that MPO-positive inflammatory cell infiltration was significantly reduced in the Amil + HS + I/R group compared to that in the HS + I/R group (Fig.3F-G). The mRNA of IL-1β, MCP-1, and TNF-α in the hepatic tissues of the Amil + HS + I/R group was significantly lower than that of the HS + I/R group (Fig.3I-K).

To declare the effect of Amil on hepatocyte apoptosis in hypernatremia liver I/R, we performed a Western blot experiment. The results showed that the addition of Amil decreases the expression of BAX, C-Caspase 3, and NLRP3 in the hepatic tissues while increasing the expression of BCL-2 (Fig.3H). TUNEL staining showed that the number of positive cells was decreased in the Amil + HS + I/R group compared to the HS + I/R group (Fig.3O-P). After the addition of Amil, the activity of GSH and SOD was increased in the hepatic tissues, while MDA content was significantly decreased (Fig.3L-N); correspondingly, the fluorescence intensity of DHE staining was significantly decreased in the Amil + HS + I/R group compared to that in the HS + I/R group (Fig.3Q-R). Therefore, Amil could attenuate hypernatremia-exacerbated hepatic IRI in Lewis rats.

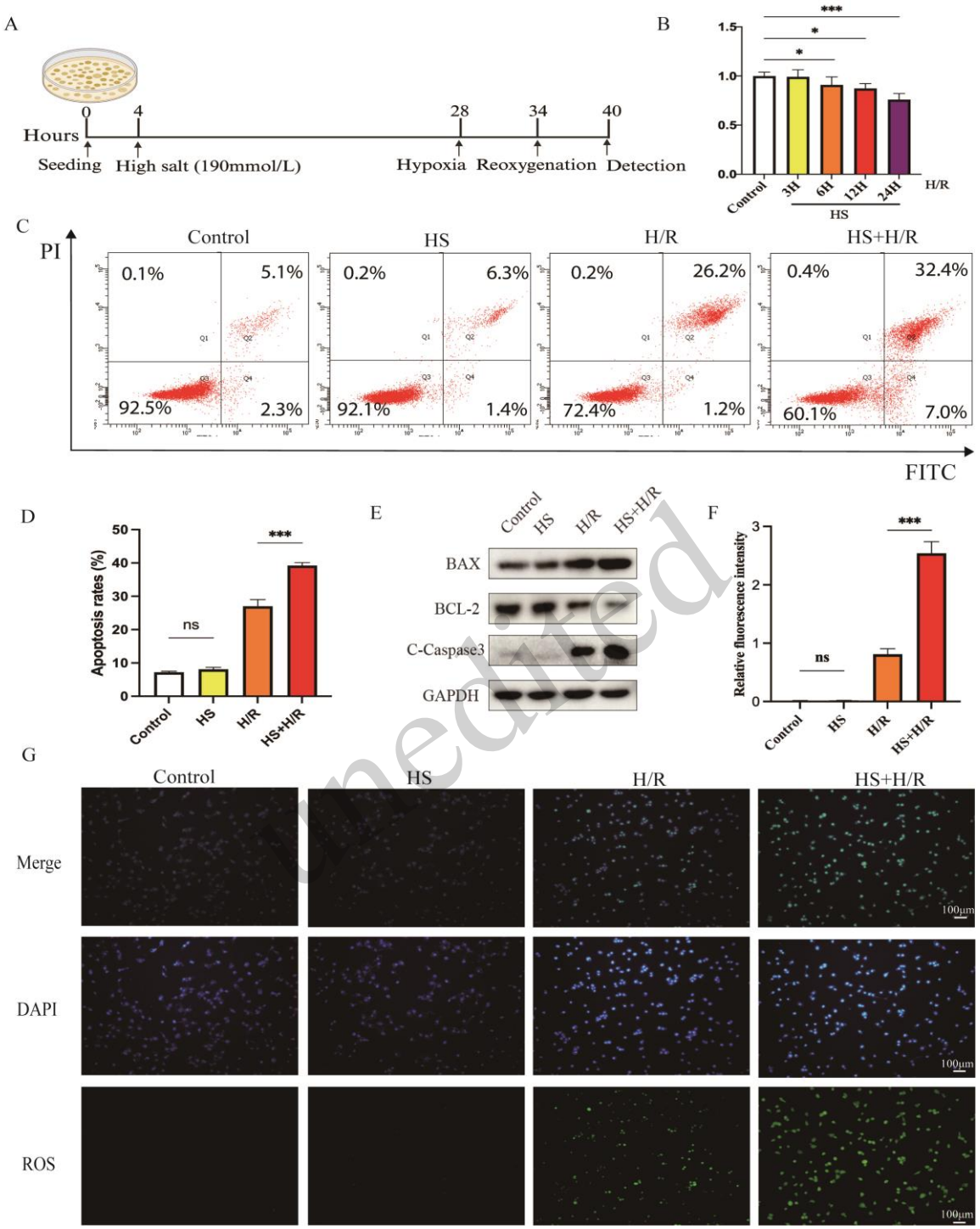


**Fig. 2 HS aggravates H/R induced injury in BRL-3A cells. (A) Flow chart for the construction of the BRL-3A cells H/R model of HS. (B) The viability of BRL-3A cells treated with 190mmol/L DMEM in different hours followed by H/R treatment was detected using CCK-8 assays. (C) Cell apoptosis rates were determined by flow cytometry and (D) statistical charts (n=4/per group). (E) The protein expression of BAX, BCL-2, and C-Caspase 3 in BRL-3A cells. (G) Representative ROS, DAPI, and merged staining images of BRL-3A cells in control, HS, H/R, and HS + H/R groups, and (F) statistical charts (n=4/per group), scale bar, 100 μm.**

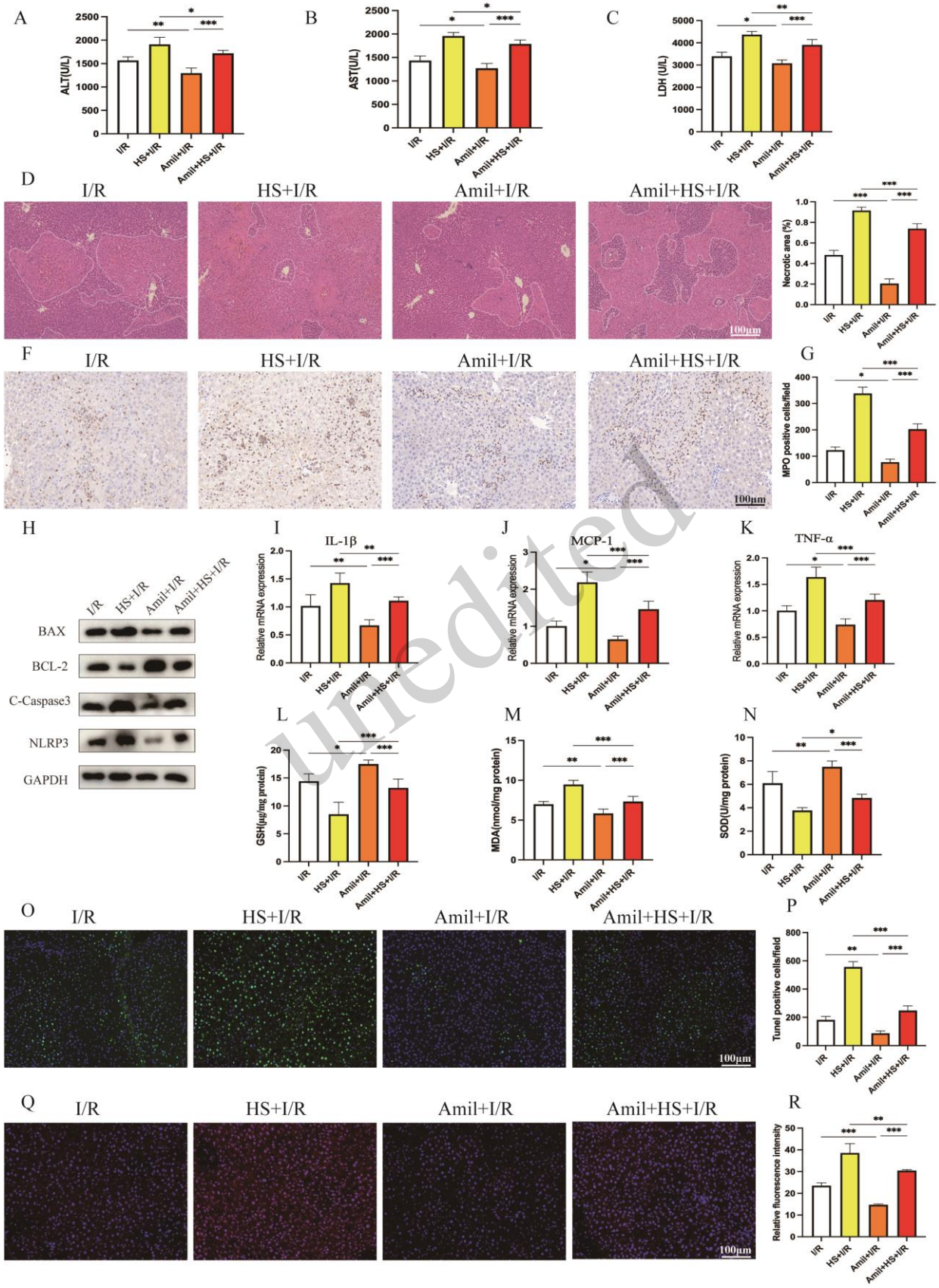
A
ALT(U/L)
B
AST(U/L)
C
LDH (U/L)
D
I/R
HS+I/R
Amil+I/R
Amil+HS+I/R
100μm
Necrotic area (%)
F
MPO positive cells/field
G
H
BAX
BCL-2
C-Caspase3
NLRP3
GAPDH
I
IL-1β
Relative mRNA expression
J
MCP-1
K
TNF-α
L
GSH(μg/mg protein)
M
MDA(nmol/mg protein)
N
SOD(U/mg protein)
O
P
Tunel positive cells/field
Q
R
Relative fluorescence intensity

**Fig. 3 Amil attenuates hypernatremia-aggravated hepatic IRI in Lewis rats. (A-C) Serum ALT, AST, and LDH levels in rats of I/R, HS + I/R, Amil + I/R, and Amil + HS + I/R groups (n=6/per group). (D) Representative hepatic H&E-stained images and (E) statistical charts (n=4/per group) showing necrotic areas, scale bar, 100 μm. (F) Representative hepatic MPO immunohistochemical staining images and (G) statistical charts (n=4/per group), scale bar, 100 μm. (H) The protein expression of BAX, BCL-2, C-Caspase 3, and NLRP3 in hepatic tissues. (I-K) The mRNA levels of IL-1β, MCP-1, and TNF-α in hepatic tissues. (L-N) Hepatic GSH activity, MDA content, and SOD activity in rats of I/R, HS + I/R, Amil + I/R, and Amil + HS + I/R groups (n=6/per group). (O) Representative hepatic TUNEL staining images and (P) statistical charts (n=4/per group), scale bar, 100 μm, (Q) Representative hepatic DHE staining images and (R) statistical charts in rats of I/R, HS + I/R, Amil + I/R, and Amil + HS + I/R groups (n=4/per group), scale bar, 100 μm.**

### 3.4 Amil attenuates HS aggravated H/R injury in BRL-3A cells.

The CCK8 results showed that, in the BRL-3A cells of the Amil + HS + H/R group, cell viability was significantly improved when the Amil concentration was 10 μmol/L. So, we used 10 μmol/L as the concentration for the Amil cell experiments (Fig.4A). Amil reduced hepatocyte apoptosis after H/R in the HS state. Flow cytometry results showed that the apoptosis rates of cells in the Amil + HS + H/R group were significantly lower than those in the HS + H/R group (Fig.4B, D). Western blot analysis showed that the expression of BAX, C-Caspase 3, and NLRP3 was decreased in the Amil + HS + H/R group compared with the HS + H/R group. In contrast, BCL-2 expression was elevated (Fig.4C). The fluorescence intensity of ROS staining was significantly lower in the Amil + HS + H/R group than in the HS + H/R group (Fig.4E-F). In conclusion, Amil could attenuate HS-exacerbated H/R injury in BRL-3A cells.

### 3.5 SN-6 attenuates hypernatremia-aggravated hepatic IRI in Lewis rats.

To study the role of NCX in hypernatremia-exacerbated hepatic IRI, we injected SN-6 into rats by intraperitoneal injection. The serum levels of ALT, AST, and LDH were significantly lower in the SN-6 + HS + I/R group than those in the HS + I/R group (Fig.5A-C). The H&E-stained images showed that the area of hepatic necrosis was decreased in the SN-6 + HS + I/R group compared with that in the HS + I/R group (Fig.5D-E). Immunohistochemical staining showed that MPO-positive inflammatory cell infiltration was significantly lower in the SN-6 + HS + I/R group (Fig.5F-G). Meanwhile, PCR results showed that the mRNA of IL-1β, MCP-1, and TNF-α was significantly lower in the SN-6 + HS + I/R group than in the HS + I/R group (Fig.5I-K).

The results of the Western blot analysis showed that the addition of SN-6 decreased the expression of BAX, C-Caspase 3, and NLRP3 and promoted the expression of BCL-2 (Fig.5H). TUNEL staining found that SN-6 could reduce the number of positive cells in the hepatic tissues (Fig.5O-P). GSH and SOD activity was higher in the SN-6 + HS + I/R group than in the HS + I/R group. The MDA content was reversed (Fig.5L-N), while the fluorescence intensity of DHE staining was lower in the SN-6 + HS + I/R group than in the HS + I/R group (Fig.5Q-R). In summary, SN-6 could alleviate hepatic IRI exacerbated by hypernatremia.

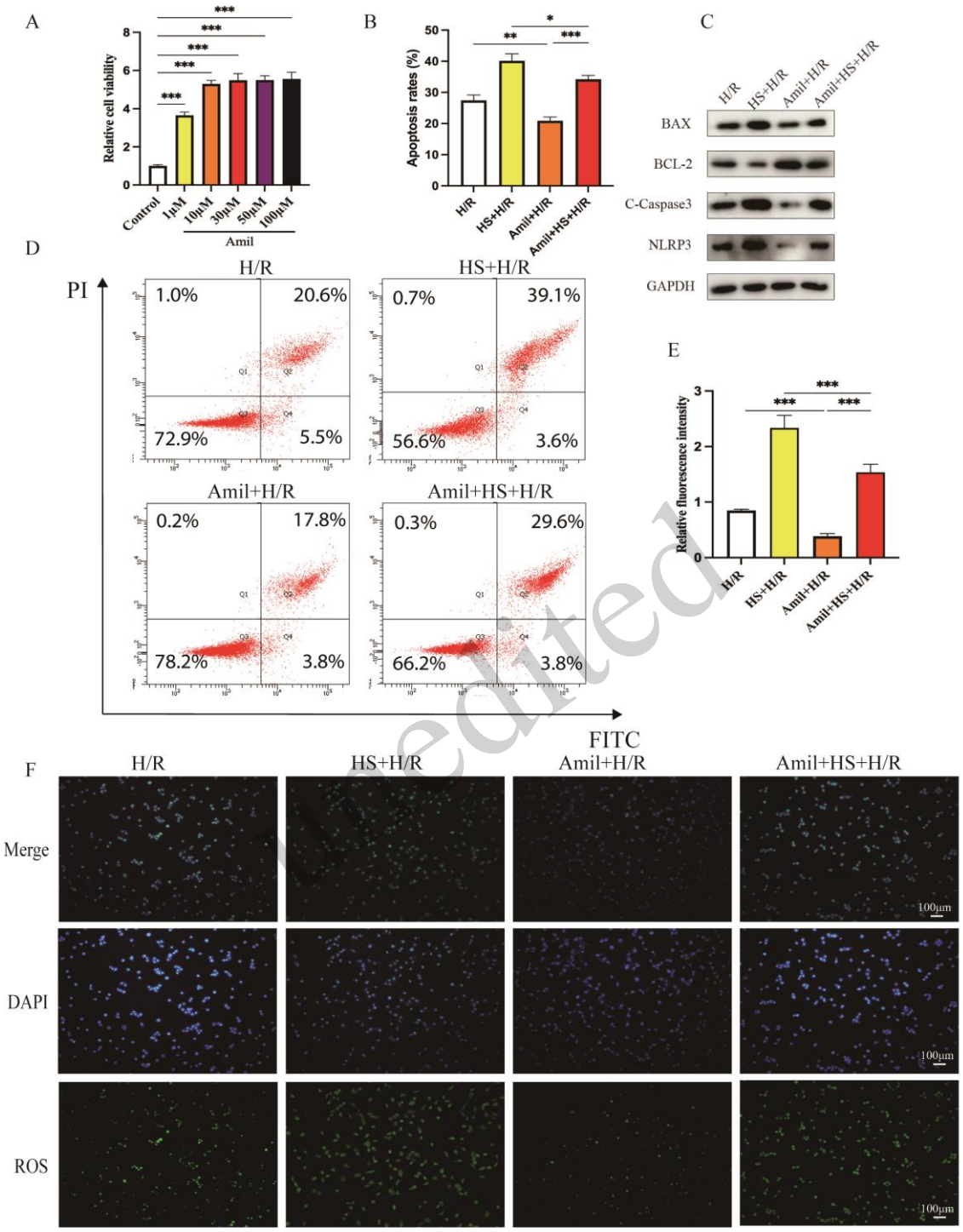


**Fig. 4 Amil attenuates HS-aggravated H/R injury in BRL-3A cells. (A) The viability of BRL-3A cells treated with different concentrations of Amil in the HS + H/R condition was detected using CCK-8 assays. (D) Cell apoptosis rates were determined by flow cytometry and (B) statistical charts (n=4/per group). (C) The protein expression of BAX, BCL-2, C-Caspase 3, and NLRP3 in BRL-3A cells. (F) Representative ROS, DAPI, and merged staining images of BRL-3A cells in H/R, HS + H/R, Amil+H/R, and Amil + HS + H/R groups, and (E) statistical charts (n=4/per group), scale bar, 100 μm.**

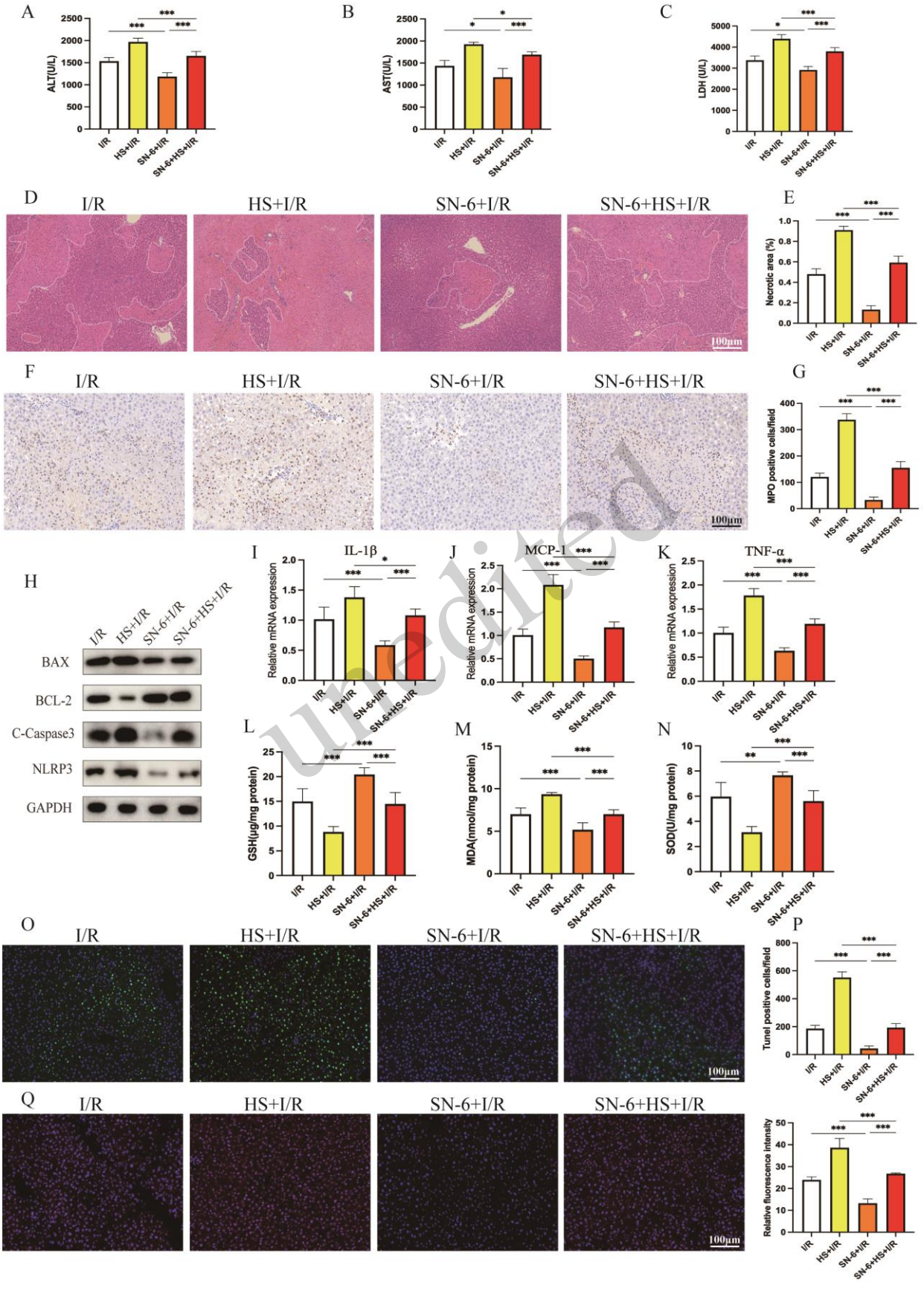
A
ALT(U/L)
B
AST(U/L)
C
LDH (U/L)
I/R
HS+I/R
SN-6+I/R
SN-6+HS+I/R
D
E
Necrotic area (%)
F
G
MPO positive cells/field
H
BAX
BCL-2
C-Caspase3
NLRP3
GAPDH
I
IL-1β
J
MCP-1
K
TNF-α
Relative mRNA expression
L
GSH(μg/mg protein)
M
MDA(nmol/mg protein)
N
SOD(U/mg protein)
O
P
Tunel positive cells/field
Q
Relative fluorescence intensity
100μm

**Fig. 5 SN-6 attenuates hypernatremia-aggravated hepatic IRI in Lewis rats. (A-C) Serum ALT, AST, and LDH levels in rats of I/R, HS + I/R, SN-6 + I/R, and SN-6 + HS + I/R groups (n=6/per group). (D) Representative hepatic H&E-stained images and (E) statistical charts (n=4/per group) showing necrotic areas, scale bar, 100 μm. (F) Representative hepatic MPO immunohistochemical staining images and (G) statistical charts (n=4/per group), scale bar, 100 μm. (H) The protein expression of BAX, BCL-2, C-Caspase 3, and NLRP3 in hepatic tissues. (I-K) The mRNA levels of IL-1β, MCP-1, and TNF-α in hepatic tissues. (L-N) Hepatic GSH activity, MDA content, and SOD activity in rats of I/R, HS + I/R, SN-6 + I/R, and SN-6 + HS + I/R groups (n=6/per group). (O) Representative hepatic TUNEL staining images and (P) statistical charts (n=4/per group), scale bar, 100 μm, (Q) Representative hepatic DHE staining images and (R) statistical charts in rats of I/R, HS + I/R, SN-6 + I/R, and SN-6 + HS + I/R groups (n=4/per group), scale bar, 100 μm.**

### 3.6 SN-6 attenuates HS aggravated H/R injury in BRL-3A cells.

We first explored the optimal experimental concentration of SN-6 using the CCK8 experiment. The results showed that the viability of HS + H/R- BRL-3A cells could be significantly improved when the concentration of SN-6 reached 10 μmol/L, so we used 10 μmol/L as the concentration for SN-6 cell experiments (Fig.6A). Then, the effect of SN-6 on hepatocyte apoptosis was further detected, Western blot analysis found that the addition of SN-6 resulted in a significant decrease of the expression of BAX, C-Caspase 3, and NLRP3. In contrast, the expression of BCL-2 was increased in the SN-6 + HS + H/R group compared with the HS + H/R group (Fig.6B). Flow cytometry results showed that the apoptosis rates were significantly decreased in the SN-6 + HS + H/R group compared with those in the HS + H/R group (Fig.6C, D). The fluorescence intensity of ROS staining in the SN-6 + HS + H/R group was significantly lower than that of the HS + H/R group (Fig.6E, F). In conclusion, SN-6 could attenuate HS-enhanced H/R injury in BRL-3A cells.

## 4 Discussion

Donors for liver transplantation are mainly patients with brain death or cardiac death. Because of excessive infusion of fluids containing sodium, increased aldosterone, and renal dysfunction, donors often suffer from hypernatremia (Ilardi, 2022; Bernal et al., 2023). Elevated donor serum sodium concentrations have been widely reported to adversely affect LT, and the results of a systematic study that included 25 study cohorts and 19,389 LT recipients suggest that donor hypernatremia is associated with poor liver function in the early postoperative period (Basmaji, et al., 2020). Livers from donors with serum sodium concentrations >155 mmol/L are considered extended-criteria donor livers with a potential risk of poor prognosis (Basmaji, et al., 2020; Mcdonald, et al., 2021). However, the molecular mechanisms underlying this clinical phenomenon remain unreported. In our study, we found that hypernatremia aggravated IRI in Lewis rat livers, and HS also aggravated H/R injury in BRL-3A cells, which was associated with ENaC and NCX; their specific inhibitors could be applied to reduce the negative effects of hypernatremia on hepatic I/R (Fig.7).

It has been widely reported that I/R increases hepatic inflammation and injury (Guo, et al., 2020; Ding, et al., 2022), and we found that hepatic IRI was further exacerbated in hypernatremia rats. We constructed the I/R model of Lewis rats with hypernatremia; the serum levels of ALT, AST, and LDH, and the area of hepatic ischemic necrosis were all significantly higher in the HS + I/R group compared to those in the I/R group. Meanwhile, inflammatory cytokines and ROS in the livers were increased in the HS + I/R group, as evidenced by an increase of IL-1β, MCP-1, TNF-α, the content of MDA, and a decrease of GSH and SOD activity(Chen et al., 2022; Han et al., 2022). Similar results were found in the BRL-3A cells assay, where the fluorescence intensity of the ROS staining of the cells in the HS + H/R group was significantly increased, and flow cytometry showed an increase in cell apoptosis. The Western blot analysis showed increased expression of BAX and

C-Caspase 3 in both the HS + I/R group of rats and the HS + H/R group of cells. Exacerbation of IRI by hypernatremia has been reported in the heart (Castaldo, et al., 2017) and kidney (Matsumoto, et al., 2022). Its molecular mechanism is related to the activation of ENaC (Matsumoto, et al., 2022) and NCX (Castaldo, et al., 2017) and leads to intracellular calcium overload and terminally exacerbates IRI. Therefore, we applied specific inhibitors of ENaC and NCX to validate their roles in hepatic IRI aggravated by hypernatremia.

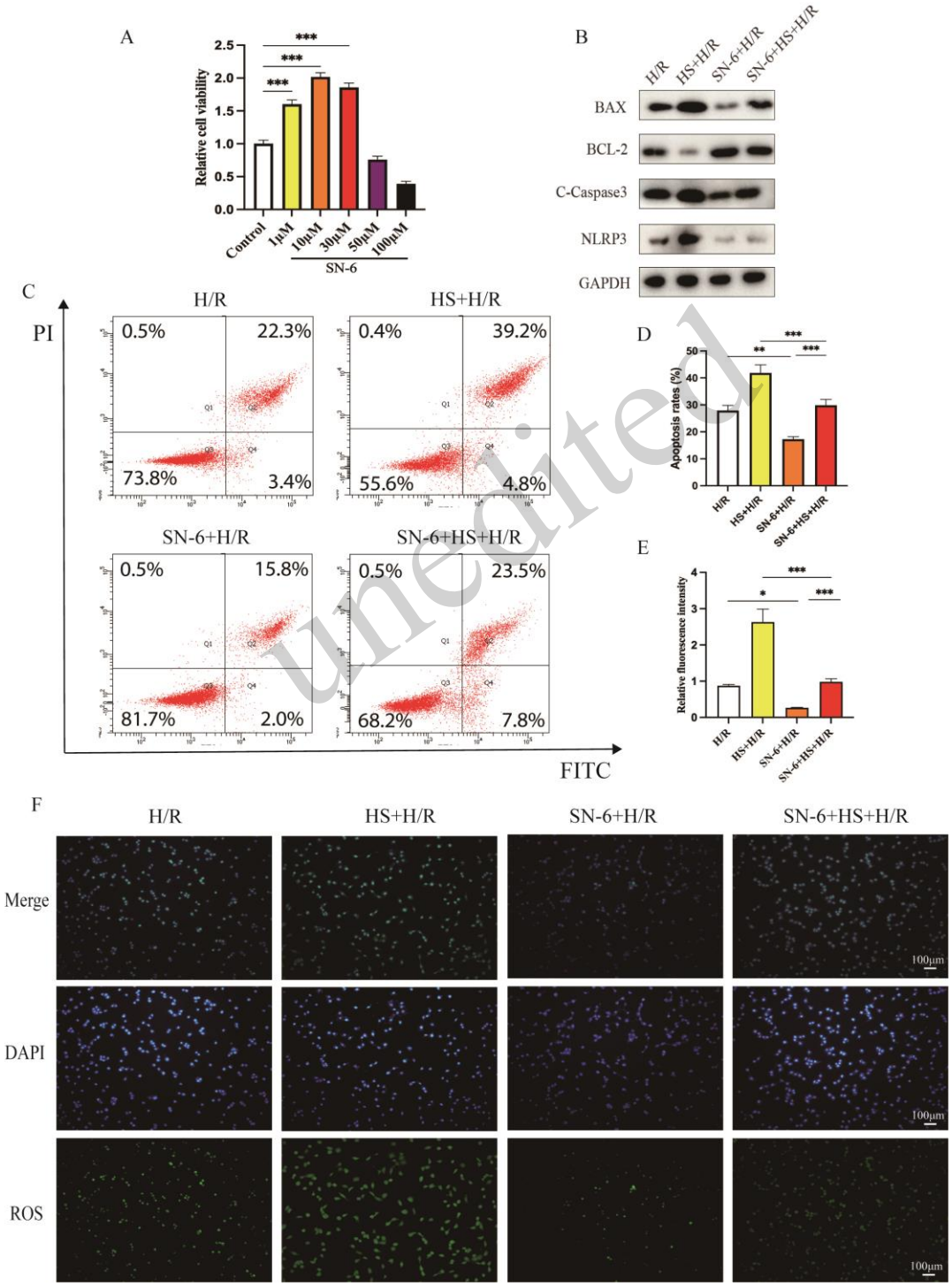

**Fig. 6 SN-6 attenuates HS aggravated H/R injury in BRL-3A cells. (A) The viability of BRL-3A cells treated with different concentrations of SN-6 in the HS + H/R condition was detected using CCK-8 assays. (B) The protein expression of BAX, BCL-2, C-Caspase 3, and NLRP3 in BRL-3A cells. (C) Cell apoptosis rates were determined by flow cytometry and (D) statistical charts (n=4/per group). (F) Representative ROS, DAPI, and merged staining images of BRL-3A cells in H/R, HS + H/R, SN-6 + I/R, and SN-6 + HS + I/R groups, and (E) statistical charts (n=4/per group), scale bar, 100 μm.**

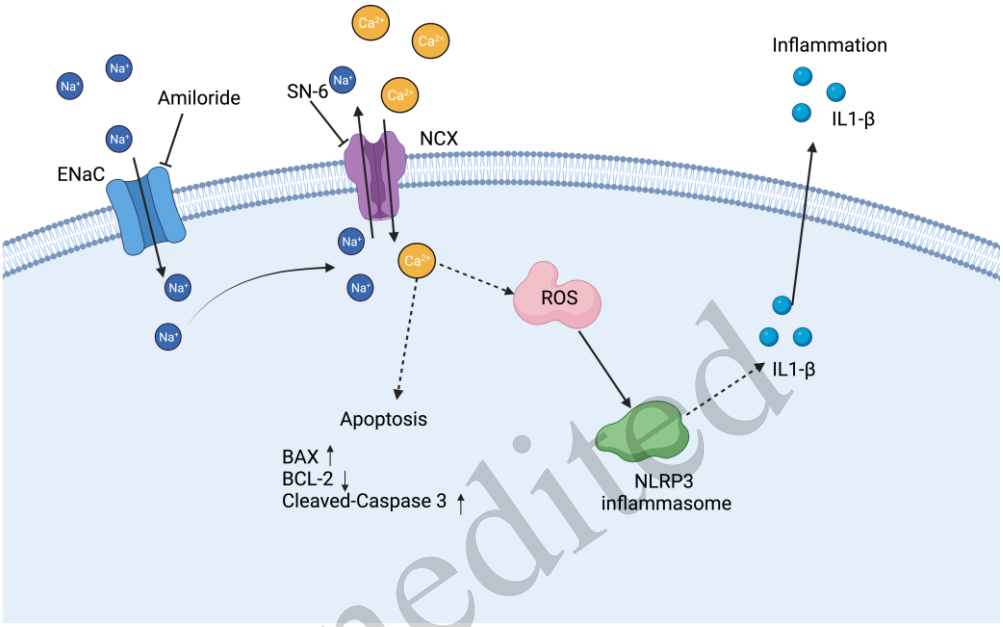




**Fig. 7 Schematic diagram of the mechanism by which hypernatremia aggravates hepatic IRI. Elevated extracellular $Na^+$ leads to the increase of the entry of $Na^+$ into the cell via ENaC. Increased intracellular $Na^+$ promotes the exchange of intracellular $Na^+$ with extracellular $Ca^{2+}$ via NCX. Intracellular $Ca^{2+}$ overload leads to increased production of ROS and NLRP3, which ultimately enhances cellular apoptosis and inflammation. The inhibitors of ENaC and NCX, Amil and SN-6, can reduce hypernatremia-aggravated hepatic IRI.**

ENaC is a kind of sodium channel that is usually composed of α, β, and γ subunits. Its main role is to maintain cellular sodium homeostasis, and it has been reported to be closely associated with ROS production in cystic fibrosis and cardiovascular sclerosis (Pitzer, et al., 2022; Chen, et al., 2023). ENaC-mediated extracellular $Na^+$ influx elevates intracellular $Na^+$, and increased exchange of $Na^+$ and $Ca^{2+}$ leads to intracellular $Ca^{2+}$ overload, which activates $Ca^{2+}$-related signaling pathways, leading to increased ROS production and inflammatory cytokines, facilitating cell apoptosis (Dizin et al., 2021; Pitzer, et al., 2022). αENaC knockout attenuated renal IRI in mice, and the application of 1 μM Amil in human microvascular endothelial cells (HMEC-1) promoted the activation of endothelial nitric oxide synthase (eNOS) (Tarjus et al., 2019). Knockout of γENaC could also increase eNOS in the kidney (Mutchler et al., 2021). $Na^+$ was enriched, and NCX activity was increased in neuronal cells after global cerebral ischemia, and neuronal cell death could be alleviated by intraperitoneal injection of Amil in a mouse model (Kang et al., 2020). In our study, we found that the application of Amil reduced hepatic inflammation and cellular apoptosis. Hepatic ROS production was decreased in the Amil + HS + I/R and Amil + HS + H/R groups. Alleviated hepatic inflammation was evidenced by reduced MPO-positive cellular infiltration and decreased IL-1β, MCP-1, and TNF-α. Inhibition of ENaC attenuated the effects of hypernatremia on hepatic IRI.

NCX mediates the cellular exchange of $Na^+$ and $Ca^{2+}$, and NCX-1 is an isoform of NCX (Xue et al., 2023). Transient ischemia led to increased $Na^+$ concentration in astrocytes, followed by increased NCX activity, to promote $Na^+$ efflux (Gerkau et al., 2018). The elevation of the $Na^+$ concentration in the perfusate from 145 to155 μmmol/L aggravated cardiac IRI, and the adverse effects caused by HS could be alleviated by the application of an inhibitor of NCX (King et al., 2020). After I/R of cardiomyocytes, NCX-1 expression was increased, and myocardial IRI was reduced after application of SN-6 (Hu et al., 2019; Li et al., 2019; Shi et al., 2023). Activation of NCX led to an increase of $Ca^{2+}$ in the cells, which in turn led to a rise in ROS production and promoted cellular inflammatory cytokines production and cellular apoptosis (Castaldo, et al., 2017). After myocardial I/R, $Na^+$ and $Ca^{2+}$ overload in cardiomyocytes led to NLRP3 activation and increased IL-1β release. Dapagliflozin inhibited the activity of NCX on cardiomyocytes, reduced intracellular $Ca^{2+}$, and decreased the inflammation and apoptosis of cardiomyocytes (Yu et al., 2021). NCX expression was increased after myocardial infarction, and rosmarinic acid prevented myocardial hypertrophy and cardiac dysfunction by inhibiting NCX (Javidanpour et al., 2018). After the application of SN-6, our study found that cellular ROS production and MPO-positive cells were reduced in SN-6 + HS + H/R groups. BAX and C-Caspase 3 expression were decreased, BCL-2 expression was increased both in SN-6 + HS + I/R and SN-6 + HS + H/R groups, and cellular apoptosis was reduced as shown by flow cytometry and TUNEL fluorescence intensity, demonstrating that SN-6 could improve HS-induced IRI.

In this study, we applied original animal and cellular models of HS. Our experiments verified that a stable 190 mmol/L serum sodium concentration rat model could be established by applying a 3 mol/L NaCl solution pumped through the tail vein. During the induction period, 0.7 ml/100 g body weight of 3 mol/L NaCl solution was first pumped through the tail vein over 5 min. Then, 0.7 ml/h of 3 mol/L NaCl solution was continuously pumped during the ascending period, and the serum sodium concentration could generally reach 190 mmol/L after 3 h. Finally, the pumping rate during the maintenance period was adjusted to 0.2 ml/h. For the HS cell model, BRL-3A cells were cultured with 190 mmol/L DMEM for 24 hours before H/R. New animal and cellular models simulate the process of LT from hypernatremia donor livers and provide tools to study the role of hypernatremia in hepatic IRI.

There are some shortcomings in our study: we did not apply gene-edited cells or animals for the study, and in addition, the rat model of hypernatremia was relatively transient because it was difficult to establish a long-term stable rat model with serum sodium concentrations up to 190 mmol/L. Therefore, it would be meaningful to apply the gene knockout or overexpression models of ENaC and NCX further for in vivo and in vitro experiments. As we know, liver sinusoidal endothelial cells (LSECs) and Kupffer cells play an important role in hepatic IRI. We speculate that the concentration of $Na^+$ and $Ca^{2+}$ in these cells will also increase under high sodium conditions, and calcium overload leads to the activation of downstream inflammation and apoptosis pathways. Therefore, to study the mechanism by which hypernatremia aggravates hepatic IRI, it will be valuable to further isolate primary LSECs and Kupffer cells for in vitro experiments.

In summary, our study demonstrated that the exacerbation of hepatic IRI by hypernatremia is related to ENaC and NCX, and that the application of the specific inhibitors Amil and SN-6 could attenuate hepatic IRI exacerbated by hypernatremia. Our conclusions suggest a new therapeutic option for hypernatremia donors and contribute to improving the utilization rate of hypernatremia donor livers.



## Data availability statement

All relevant data are included in the article and supplementary material. For further inquiries, please refer to the detailed information in the following websites (https://www.springer.com/us/editorial-policies/data-availability-statement; https://www.springernature.com/gp/authors/research-data-policy/data-availability-statements)

## Acknowledgments

This work was supported by Funding for Scientific Research and Innovation Team of The First Affiliated Hospital of Zhengzhou University (No. ZYCXTD2023007).

## Author contributions

Wenzhi GUO, and Yabin CHEN designed the experiments. Yabin CHEN, Peihao WEN and Hao LI performed the experiments. Jiakai ZHANG and Zhihui WANG analyzed the data and wrote the manuscript. Shengli CAO edited the gramma. All authors read and approved the final manuscript, and therefore, had full access to all the data in the study and take responsibility for the integrity and security of the data.

## Compliance with ethics guidelines

Yabin CHEN, Hao LI, Peihao WEN, Jiakai ZHANG, Zhihui WANG, Shengli CAO, and Wenzhi GUO declare that they have no conflict of interest.

This study was approved by the Clinical Research Ethics Committee of the First Affiliated Hospital of Zhengzhou University (Ref: 2023-KY-0006). All rats were cared in accordance with the Guide for the Care and Use of Laboratory Animals. All procedures followed were in accordance with the ethical standards of the Helsinki Declaration of 1975, as revised in 2008 (5).

## References

Basmaji J, Hornby L, Rochwerg B, et al., 2020. Impact of donor sodium levels on clinical outcomes in liver transplant recipients: A systematic review. *Eur J Gastroenterol Hepatol*, 32(12):1489-1496. https://doi.org/10.1097/MEG.0000000000001776

Bastos-Neves D, Salvalaggio PRO, Almeida MD, 2019. Risk factors, surgical complications and graft survival in liver transplant recipients with early allograft dysfunction. *Hepatobiliary Pancreat Dis Int*, 18(5):423-429. https://doi.org/10.1016/j.hbpd.2019.02.005

Bernal A, Zafra MA, Simón MJ, et al., 2023. Sodium homeostasis, a balance necessary for life. *Nutrients*, 15(2) https://doi.org/10.3390/nu15020395

Castaldo P, Macri ML, Lariccia V, et al., 2017. Na(+)/ca(2+) exchanger 1 inhibition abolishes ischemic tolerance induced by ischemic preconditioning in different cardiac models. *Eur J Pharmacol*, 794:246-256. https://doi.org/10.1016/j.ejphar.2016.11.045

Ceresa CDL, Nasralla D, Pollok JM, et al., 2022. Machine perfusion of the liver: Applications in transplantation and beyond. *Nat Rev Gastroenterol Hepatol*, 19(3):199-209. https://doi.org/10.1038/s41575-021-00557-8

Chen Q, Li Q, Liang Y, et al., 2022. Natural exosome-like nanovesicles from edible tea flowers suppress metastatic breast cancer via ros generation and microbiota modulation. *Acta Pharm Sin B*, 12(2):907-923. https://doi.org/10.1016/j.apsb.2021.08.016

Chen SY, Zhang HP, Li J, et al., 2021. Tripartite motif-containing 27 attenuates liver ischemia/reperfusion injury by suppressing transforming growth factor beta-activated kinase 1 (tak1) by tak1 binding protein 2/3 degradation. *Hepatology*, 73(2):738-758. https://doi.org/10.1002/hep.31295

Chen Y, Yu X, Yan Z, et al., 2023. Role of epithelial sodium channel-related inflammation in human diseases. *Front Immunol*, 14:1178410. https://doi.org/10.3389/fimmu.2023.1178410

Dar WA, Sullivan E, Bynon JS, et al., 2019. Ischaemia reperfusion injury in liver transplantation: Cellular and molecular mechanisms. *Liver Int*, 39(5):788-801. https://doi.org/10.1111/liv.14091

Ding MJ, Fang HR, Zhang JK, et al., 2022. E3 ubiquitin ligase ring finger protein 5 protects against hepatic ischemia reperfusion injury by mediating phosphoglycerate mutase family member 5 ubiquitination. *Hepatology*, 76(1):94-111. https://doi.org/10.1002/hep.32226

Dizin E, Olivier V, Roth I, et al., 2021. Activation of the hypoxia-inducible factor pathway inhibits epithelial sodium channel-mediated sodium transport in collecting duct principal cells. *J Am Soc Nephrol*, 32(12):3130-3145. https://doi.org/10.1681/ASN.2021010046

Frindt G, Yang L, Bamberg K, et al., 2018. Na restriction activates epithelial na channels in rat kidney through two mechanisms and decreases distal na(+) delivery. *J Physiol*, 596(16):3585-3602. https://doi.org/10.1113/JP275988

Gerkau NJ, Rakers C, Durry S, et al., 2018. Reverse ncx attenuates cellular sodium loading in metabolically compromised cortex. *Cereb Cortex*, 28(12):4264-4280. https://doi.org/10.1093/cercor/bhx280

Guo WZ, Fang HB, Cao SL, et al., 2020. Six-transmembrane epithelial antigen of the prostate 3 deficiency in hepatocytes protects the liver against ischemia-reperfusion injury by suppressing transforming growth factor-beta-activated kinase 1. *Hepatology*, 71(3):1037-1054. https://doi.org/10.1002/hep.30882

Guo Z, Zhao Q, Jia Z, et al., 2023. A randomized-controlled trial of ischemia-free liver transplantation for end-stage liver disease. *J Hepatol*, 79(2):394-402. https://doi.org/10.1016/j.jhep.2023.04.010

Han M, Lin J, Yang Y, et al., 2022. Xinshuaining preparation protects h9c2 cells from h(2)o(2)-induced oxidative damage through the pi3k/akt/nrf-2 signaling pathway. *Clin Exp Hypertens*, :1-9. https://doi.org/10.1080/10641963.2022.2131806

Hu HJ, Wang SS, Wang YX, et al., 2019. Blockade of the forward na(+) /ca(2+) exchanger suppresses the growth of glioblastoma cells through ca(2+) -mediated cell death. *Br J Pharmacol*, 176(15):2691-2707. https://doi.org/10.1111/bph.14692

Ilardi A, 2022. Diagnostic and therapeutic approach to hypernatremia. *Diagnosis (Berl)*, 9(4):403-410. https://doi.org/10.1515/dx-2022-0034

Javidanpour S, Dianat M, Badavi M, et al., 2018. The inhibitory effect of rosmarinic acid on overexpression of ncx1 and stretch-induced arrhythmias after acute myocardial infarction in rats. *Biomed Pharmacother*, 102:884-893.

https://doi.org/10.1016/j.biopha.2018.03.103
Kaltenmeier C, Yazdani HO, Handu S, et al., 2022. The role of neutrophils as a driver in hepatic ischemia-reperfusion injury and cancer growth. *Front Immunol*, 13:887565. https://doi.org/10.3389/fimmu.2022.887565
Kang BS, Choi BY, Kho AR, et al., 2020. An inhibitor of the sodium-hydrogen exchanger-1 (nhe-1), amiloride, reduced zinc accumulation and hippocampal neuronal death after ischemia. *Int J Mol Sci*, 21(12) https://doi.org/10.3390/ijms21124232
King DR, Padget RL, Perry J, et al., 2020. Elevated perfusate [na(+)] increases contractile dysfunction during ischemia and reperfusion. *Sci Rep*, 10(1):17289. https://doi.org/10.1038/s41598-020-74069-x
Li J, Yu D, He C, et al., 2023. Klf6 alleviates hepatic ischemia-reperfusion injury by inhibiting autophagy. *Cell Death Dis*, 14(7):393. https://doi.org/10.1038/s41419-023-05872-3
Li Y, Quan X, Li X, et al., 2019. Kdm6a protects against hypoxia-induced cardiomyocyte apoptosis via h3k27me3 demethylation of ncx gene. *J Cardiovasc Transl Res*, 12(5):488-495. https://doi.org/10.1007/s12265-019-09882-5
Lin Y, Huang H, Chen L, et al., 2023. Assessing donor liver quality and restoring graft function in the era of extended criteria donors. *J Clin Transl Hepatol*, 11(1):219-230. https://doi.org/10.14218/JCTH.2022.00194
Lucas-Ruiz F, Mateo SV, Jover-Aguilar M, et al., 2023. Danger signals released during cold ischemia storage activate nlrp3 inflammasome in myeloid cells and influence early allograft function in liver transplantation. *EBioMedicine*, 87:104419. https://doi.org/10.1016/j.ebiom.2022.104419
Matsumoto T, Doi S, Nakashima A, et al., 2022. Upregulation of mineralocorticoid receptor contributes to development of salt-sensitive hypertension after ischemia-reperfusion injury in rats. *Int J Mol Sci*, 23(14) https://doi.org/10.3390/ijms23147831
Mcdonald MF, Barrett SC, Malik TH, et al., 2021. Elevated serum sodium in recipients of liver transplantation has a substantial impact on outcomes. *Transpl Int*, 34(10):1971-1983. https://doi.org/10.1111/tri.13968
Mutchler SM, Hasan M, Kohan DE, et al., 2021. Deletion of the gamma subunit of enac in endothelial cells does not protect against renal ischemia reperfusion injury. *Int J Mol Sci*, 22(20) https://doi.org/10.3390/ijms222010914
N'gouemo P, 2013. Probing the role of the sodium/calcium exchanger in pentylenetetrazole-induced generalized seizures in rats. *Brain Res Bull*, 90:52-57. https://doi.org/10.1016/j.brainresbull.2012.09.007
Persaud A, Jiang C, Liu Z, et al., 2022. Elevated intracellular na(+) and osmolarity stimulate catalytic activity of the ubiquitin ligase nedd4-2. *Proc Natl Acad Sci U S A*, 119(30):e2122495119. https://doi.org/10.1073/pnas.2122495119
Pitzer A, Elijovich F, Laffer CL, et al., 2022. Dc enac-dependent inflammasome activation contributes to salt-sensitive hypertension. *Circ Res*, 131(4):328-344. https://doi.org/10.1161/CIRCRESAHA.122.320818
Quansah H, N'gouemo P, 2014. Amiloride and sn-6 suppress audiogenic seizure susceptibility in genetically epilepsy-prone rats. *CNS Neurosci Ther*, 20(9):860-866. https://doi.org/10.1111/cns.12296
Scambler T, Jarosz-Griffiths HH, Lara-Reyna S, et al., 2019. Enac-mediated sodium influx exacerbates nlrp3-dependent inflammation in cystic fibrosis. *Elife*, 8 https://doi.org/10.7554/eLife.49248
Schlegel A, Mueller M, Muller X, et al., 2023. A multicenter randomized-controlled trial of hypothermic oxygenated perfusion (hope) for human liver grafts before transplantation. *J Hepatol*, 78(4):783-793. https://doi.org/10.1016/j.jhep.2022.12.030
Shi X, Yin Y, Guo X, et al., 2023. The histone deacetylase inhibitor saha exerts a protective effect against myocardial ischemia/reperfusion injury by inhibiting sodium-calcium exchanger. *Biochem Biophys Res Commun*, 671:105-115. https://doi.org/10.1016/j.bbrc.2023.05.120
Sitbon A, Delmotte PR, Goumard C, et al., 2023. Therapeutic potentials of mesenchymal stromal cells-derived extracellular vesicles in liver failure and marginal liver graft rehabilitation: A scoping review. *Minerva Anestesiol*, 89(7-8):690-706. https://doi.org/10.23736/S0375-9393.23.17265-8
Tarjus A, Gonzalez-Rivas C, Amador-Martinez I, et al., 2019. The absence of endothelial sodium channel alpha (alphaenac) reduces renal ischemia/reperfusion injury. *Int J Mol Sci*, 20(13) https://doi.org/10.3390/ijms20133132
Xue J, Zeng W, Han Y, et al., 2023. Structural mechanisms of the human cardiac sodium-calcium exchanger ncx1. *Nat Commun*, 14(1):6181. https://doi.org/10.1038/s41467-023-41885-4
Yu YW, Que JQ, Liu S, et al., 2021. Sodium-glucose co-transporter-2 inhibitor of dapagliflozin attenuates myocardial ischemia/reperfusion injury by limiting nlrp3 inflammasome activation and modulating autophagy. *Front Cardiovasc Med*, 8:768214. https://doi.org/10.3389/fcvm.2021.768214
Zhou ZJ, Chen GS, Si ZZ, et al., 2020. Prognostic factors influencing outcome in adult liver transplantation using hypernatremic organ donation after brain death. *Hepatobiliary Pancreat Dis Int*, 19(4):371-377. https://doi.org/10.1016/j.hbpd.2020.06.003

**Supplementary information**

Tables S1 and S2